# Spatial dependence of surface error slopes on tolerancing panoramic lenses

Jocelyn Parent and Simon Thibault*

Centre for Optics, Photonics and Laser, Laval University, Québec City, Québec, Canada, G1V 0A6

*Corresponding author: simon.thibault@phy.ulaval.ca

Received 2 February 2010; revised 20 April 2010; accepted 20 April 2010;
posted 20 April 2010 (Doc. ID 123680); published 7 May 2010

Surface irregularity errors are conventionally used to specify fabrication accuracy of spherical, aspheric, or plane surfaces. However, in some cases, the amplitude of the irregularities fails to fully describe the surface accuracy requirement when the pupil size is small compared to the surface diameter. In such cases, the irregularity slope will induce distortion. A spatially dependent representation of the irregularity slope is proposed and implemented to specify the surface accuracy. As an optical design example, we study in detail the case of the front surfaces of a fish-eye lens and a panomorph lens. Panoramic lenses are characterized by a small entrance pupil and by important distortion. For both lenses, we found that the novel field-dependent mathematical descriptor provided a nearly perfect agreement with Monte Carlo analyses and can be used to specify the spatially dependent irregularity requirement. The approach is not limited to wide-angle lenses. 

*OCIS codes:* 080.2740, 110.3000, 220.1010, 220.3620.

## 1. Introduction

Panoramic imaging is of growing importance in many applications around the world. Obvious areas of application for panoramic lenses are in robotics and surveillance. While primarily valued for their ability to image a very large field of view (180°× 360°, hemispheric), other characteristics, such as the ability to use the captured images to make range estimations [1], stereo images [2], and three-dimensional reconstruction, are also important benefits of panoramic imaging systems in the robotic field. In surveillance, to be effective, the panoramic images are displayed in one or more unwrapped views that reproduce real-world proportions and geometric information to the human operator. Consequently, for these applications, in which we need the exact angular position of points on the object hemisphere, it is particularly important to calibrate the panoramic lens in terms of image height ($H$) and field of view ($\theta$) [3].

For a single lens unit, such a calibration can manually be achieved and the unwrapping can then be done using a lookup table, associating each image pixel to an object angle. However, the use of panoramic lenses for endoscopy, automotive applications, and surveillance calls for the calibration to be done during the design part.

A simple approach to study how surface defects will impact the image is to perform a sensitivity or inverse sensitivity tolerance analysis on the lens. This method, well developed in lens design, is useful in the production of more standard lenses, but is not well suited to panoramic lenses. This is mainly because tolerance specifications work well when all lens surfaces are entirely illuminated by the light beam coming from each field point. However, for particular lenses, when the external optical surfaces are far from the aperture stop and/or the entrance/exit pupils are small compared to the surface diameter, the surface irregularity will induce an optical path difference wavefront error that is independent of the surface RMS irregularity value [4] and will, rather, produce distortion. In this case, better tolerancing specifications have to be used, combining both the image quality and the distortion effects. This type

0003-6935/10/142686-08$15.00/0

of effect is often, but not exclusively, found in the first few surfaces of wide-angle lenses.

In this paper, we analyze the effects on the image height ($H$) of the irregularity surface errors (IRR) on the front surfaces of panoramic lens designs and, particularly, the localized surface errors. We perform standard tolerance analysis that demonstrates the problematic. We develop, in Subsection 3.A, a model to describe this impact on the image deformation based on the characteristics of the lens design. We then apply our techniques on two particular wide-angle lenses. Finally, we present guidelines that can be used to define appropriate surface irregularity tolerances for the front lens of a panoramic lens based on the tolerance margin of the designed calibration function of the lens.

## 2. Description of the Problematic

### A. Lenses with Small Beam Diameter to Lens Diameter Ratio

Figure 1 shows a panoramic lens, which is commonly called a fish-eye lens (FEL). This FEL is composed of nine spherical lenses, including two doublets. Figure 2 shows a panomorph lens (PML) [5] composed of 12 lenses with an aspheric lens front element. In both cases, the lenses have been designed for the visible waveband with a FOV of 180°, an $f$-number of 2.8, and an image plane corresponding to a 1/3 in. detector. As can be seen in these figures, a bundle of rays from a given object point is compacted closely around the chief ray on the first few surfaces of both lenses. This is often seen on surfaces that are far away from the aperture stop of the optical system, like front lenses in object space or field flatteners in image space. Lenses with a limited field of view can have this characteristic [6], but it is more problematic near the front elements of wide-angle lenses, as discussed in Subsection 4.B.

### B. Localized Surface Errors

The sensitivity of wide-angle lenses has been reported in the past [7,8]. Recently, we reported new

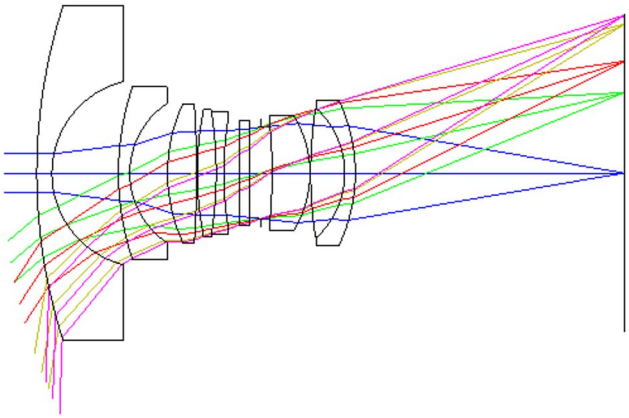

Fig. 1. (Color online) In this layout of a fish-eye lens (FEL), the small entrance pupil diameter compared to the front lens diameter is visible.

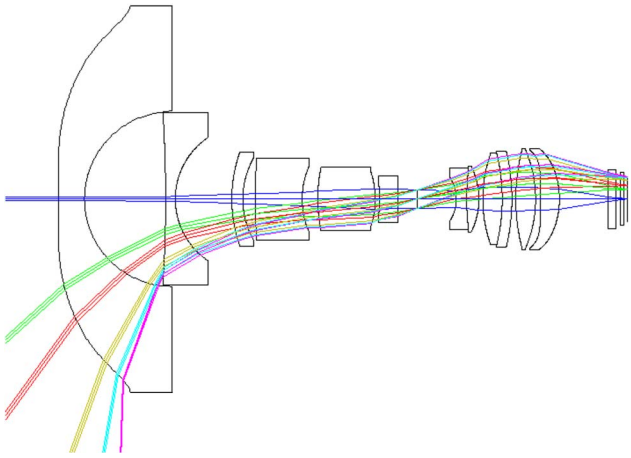

Fig. 2. (Color online) In this layout of a panomorph lens (PML), the very small entrance pupil diameter compared to the front lens diameter is even more critical than in the FEL.

observations on the behavior of those lenses under perturbation, which indicates that a careful investigation during the design phase is inevitable in order to predict the image deformation under perturbation. The impact of IRR period and amplitude has been studied on aspheric lenses [9], as well as the RMS IRR gradient [10]. However, none of these studies reported that the IRR slope and amplitude can have an impact that depends on the position of this error on the surface.

To illustrate this, we consider a Gaussian-shaped error that is small compared to the surface, but large compared to the footprint. This error will not scatter the rays, but the Gaussian bump will introduce a general ray deviation. Since the error is larger that the beam footprint, the Gaussian shape can be treated as an optical surface that introduces wavefront tilt, defocus, astigmatism, etc. For our study, the tilt on the wavefront is the parameter that has an impact on the calibration because it will produce an image deformation or a variation on the image height ($\Delta H$). This is the kind of image impact previously seen in real constructed optical systems in which the entrance pupil-diameter-to-surface-diameter ratio is small [6].

Because these localized errors can have a bigger impact on the imaging quality at some surfaces than others, it is important to analyze their impact more thoroughly. This is especially true with aspheric surfaces because their sag is often described as a power series expansion, oscillating around the perfect desired surface [9,11]. The previous reported approach of using a high sampling grid sag to add Gaussian error to a surface and checking the effects on the image, as described in [8], is long and provides only part of the required information. The results are reproduced in Fig. 3 to allow later comparison in Subsection 4.B. The figure presents the variation of image height $\Delta H$ for the error positioned at various field angles, each color representing a different position. The changing amplitude of the curves in this graph

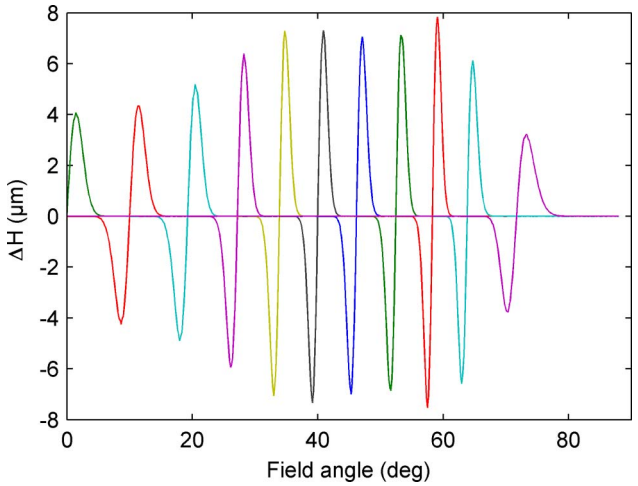


Fig. 3. (Color online) Image displacement $\Delta H$ is not constant when a Gaussian-shaped localized error is placed at different positions on the front surface of the PML. Each curve of a different color represents a different position of this error. The effect appears to be worse between 30° and 70° because the produced displacements are larger. On each curve, the maximum and minimum are located at the position of the largest positive and negative slopes in the Gaussian errors.

show that the image deformation associated with the Gaussian error varies spatially with the position on the front surface of the lens.

From a lens design point of view, a standard approach is to superpose Monte-Carlo-generated errors on the surface by using the standard Zernike model. The model is used to analyze random irregular deviations of small amplitude on a surface. Figure 4 shows, for 20 Monte Carlo runs, the changes relative to the original lens in the image in terms of the derivative function $\partial H/\partial\theta$. With $H$ on the detector converted in pixels, this function can be directly related to a measure of angular resolution in pixels/radian at a given object field angle. This resolution is related only to the angular spreading in the image, independent of image blur produced by aberrations. A deeper meaning of this $\partial H/\partial\theta$ will be presented in Subsection 3.A. Each Monte Carlo run, generated using the TEZI tolerancing function in Zemax, superposes to the ideal surface a $\Delta Z$ corresponding to some random values of Zernike polynomials up to term 37, which represents low-frequency errors. These random polynomials are then normalized to give constant amplitude of 50 $\mu$m, a value representative of the possible defects. It can be seen that, for random errors between a field angle of 30° and 70°, the impacts on the image appear to be worse because the amplitude is higher. This result indicates that the deformation produced by the IRR error is not uniform along the entire field of view. In comparison, a distortion-free lens should give a constant variation over the whole field of view for random polynomials. While this approach shows in which regions errors are more critical, it does not allow easy inversion of these results to find a maximal surface error for a required image maximal perturbation. We propose in the next section an analytical model to explain the dependence within the field of view of IRR errors.

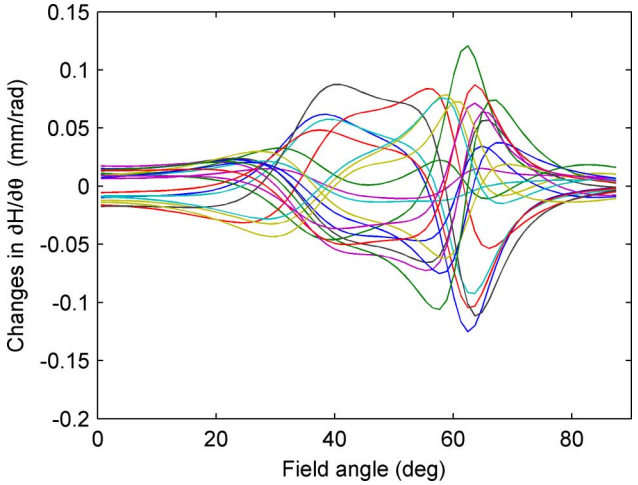


Fig. 4. (Color online) Monte-Carlo-generated error surfaces on the front surface of the PML. Each different curve represents a different Monte Carlo trial. It appears that the maximum change in resolution occurs between 30° and 70° because the changes are larger in that region.

## 3. Modeling the Surface Errors

### A. Approximating Errors as Small Wedges

As explained in Subsection 2.B, a localized surface error on a surface where the beam is small compared to this error will produce a deviation of all the rays for a given field angle. Since we are looking for the maximum deviation, the curvature of the surface error is considered negligible in the small area where rays for a given field angle hit the front surface. In fact, the maximum deviation that produces the maximum image deformation will be related to the maximum surface error slope. This means that the surface error on a refractive surface can be well approximated by a small wedge or prism, with a vertex angle $\alpha$ representing the surface error slope at a given field angle. To obtain an equation relating the displacements in the image plane to the surface errors, three important factors have to be considered in the following three steps. Figure 5 shows a schematic of the problem with the variables used.

The first step is to calculate this prism vertex angle $\alpha$ between the ideal surface and the imperfect one. To simplify, only one of the two dimensions of the surface of the lens is considered: the radial axis $Y$. Surface errors or surface accuracy, as well as surface IRR, are measured relative to the desired surface profile. When the real surface is written like $Z_{\text{real}} = Z_{\text{ideal}} + Z_{\text{error}}$, direct trigonometry shows that the real angle is $\arctan(\partial Z_{\text{real}}/\partial Y)$ and that the perfect one would be $\arctan(\partial Z_{\text{ideal}}/\partial Y)$. The difference is then directly given by Eq. (1), where $\partial Z_{\text{ideal}}/\partial Y$ is calculated from the normal of the surface by $\tan(\varphi_N)$, where the normal angle $\varphi_N$ is measured before adding the error

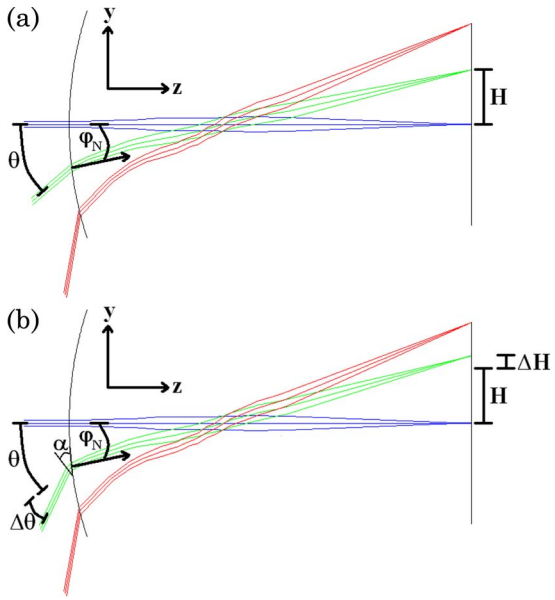


Fig. 5. (Color online) Schematic of (a) before and (b) after a surface error approximated by a prism of vertex angle $\alpha$ modifies the object angle $\theta$ and the image height $H$.

$$\alpha = \arctan(\partial Z_{\text{ideal}}/\partial Y) - \arctan(\partial Z_{\text{ideal}}/\partial Y + \partial Z_{\text{error}}/\partial Y). \quad (1)$$

For small values of $\partial Z_{\text{error}}/\partial Y$ and using the derivative of arctangent, we have

$$\alpha \approx [\partial Z_{\text{error}}/\partial Y]/[1 + \tan^2(\varphi_N)]. \quad (2)$$

This last equation shows that, for small field angles, where the surface normal is close to the optical axis, this first step could be ignored, but also that it could produce a factor of 2 where the normal angle is as high as 45°. Choosing an error normal to the surface instead of along the $Z$ axis would remove this effect.

The next step is to relate the variation of angle $\Delta\theta$ in the rays caused by a small prism. From the Snell–Descartes law of refraction, this deviation is given by Eq. (3), where $n$ is the index of refraction of the front lens and $\varphi_N$ is the normal angle independent of any added error [12]:

$$\Delta\theta = (\theta - \varphi_N) - \alpha + \arcsin[(n^2 - \sin^2(\theta - \varphi_N))^{1/2}\sin(\alpha) - \cos(\alpha)\sin(\theta - \varphi_N)]. \quad (3)$$

If the wedge angle is small, by using series expansion of the angle of incidence $(\theta - \varphi_N)$, Eq. (3) reduces to

$$\Delta\theta \approx \alpha(n-1)[1 + (\theta - \varphi_N)^2(n+1)/(2n) + (\theta - \varphi_N)^4(n+1)(5n^2+3)/(24n^3) + \ldots]. \quad (4)$$

The terms in $(\theta - \varphi_N)^{2i}$ can be neglected for small incident angles compared to the normal, but can become important in some wide-angle lenses. Depending on the maximum value of $(\theta - \varphi_N)$ in a particular lens, Eq. (3) or Eq. (4) can be used.

Finally, we use a local focal length, which depends on the field angle. For most imaging systems, the link between the field angle $\theta$ of the object and the final height $H$ in the image plane is $H = F\tan(\theta)$, where $F$ is the paraxial focal length of the system. Deviation from this equation is often called distortion. However, for some systems, such as wide-angle lenses, with field angles sometimes over 90°, this relationship does not hold. For this reason, it is more convenient in some other systems, such as in the FEL presented in this paper, to design the lens to follow an equation such as $H = F\theta$. However, this is not enough in some systems, such as the PML. In this case, a better way of writing it is Eq. (5), meaning that $H$ is a general continuous function written as a power series expansion of the field angle $\theta$. The value of $a$ is null when the 0° object is imaged at the center of the detector:

$$H = a + b\theta + c\theta^2 + d\theta^3 + \ldots O(\theta^4). \quad (5)$$

Using this, the local focal length is defined as $f(\theta) \equiv \partial H/\partial\theta$ and this is directly related to a measurement of the resolution of the system at each field angle. This resolution is often a design parameter known to the designer from the beginning of the process. Of course, in the paraxial region, where values of $\theta$ (measured in radians) are small, $f(\theta) \cong b$ and it gives back the paraxial focal length $F$ of the system. Using the definition $f(\theta) \equiv \partial H/\partial\theta$ of the local focal length, Eq. (6) is obtained:

$$\Delta H = f(\theta)\Delta\theta. \quad (6)$$

By putting Eq. (2) into Eq. (4), and then Eq. (4) into Eq. (5), the complete equation is obtained. For small surface errors, this can be written as a linear function of this error $\partial Z_{\text{error}}/\partial Y$ using the previous approximations:

$$\Delta H \approx f(\theta)/[1 + \tan^2(\varphi_N)] \times (n-1)[1 + (\theta - \varphi_N)^2(n+1)/(2n) + \ldots] \times \partial Z_{\text{error}}/\partial Y. \quad (7)$$

This equation holds for the first surface, but similar treatment could be done on other surfaces and will be discussed in Subsection 4.B.

### B. Optical Design Examples

The two wide-angle lenses shown earlier in Figs. 1 and 2 can now be analyzed using the above model. First, for the FEL, the local focal length is obtained from the lens design software and presented at Fig. 6(a). It shows that, for the FEL, the resolution tends to decrease with increasing field of view. Also, from the layout of Fig. 1, for an increasing field angle, the incident angle compared to the normal $(\theta - \varphi_N)$ is

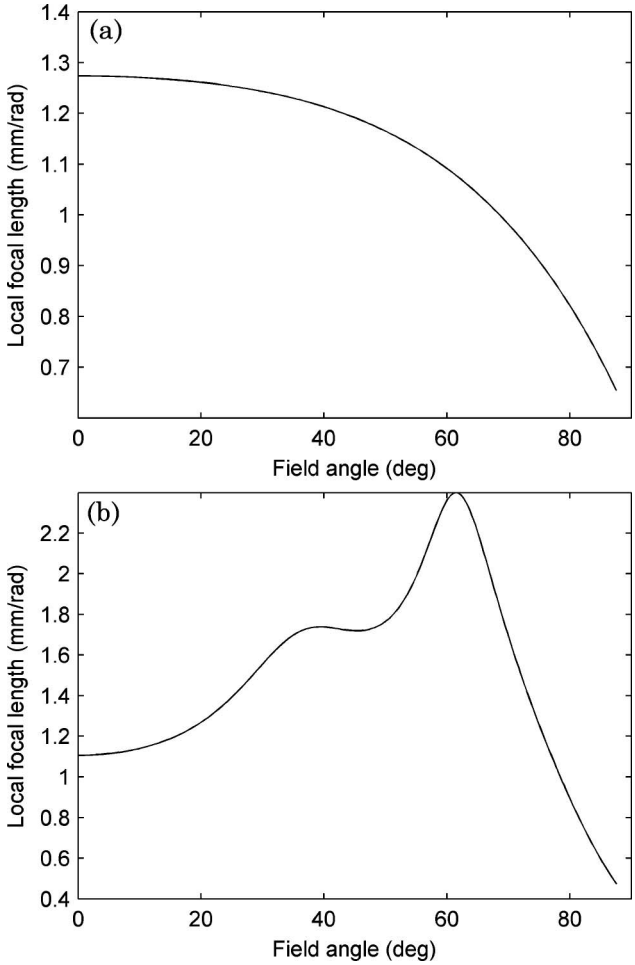


Fig. 6. Local focal length $f(\theta) \equiv \partial H/\partial\theta$. (a) For the FEL, the resolution decreases with the field angle. (b) For the PML, the resolution increases with the field angle, up to a maximum of around 63° before falling back down.

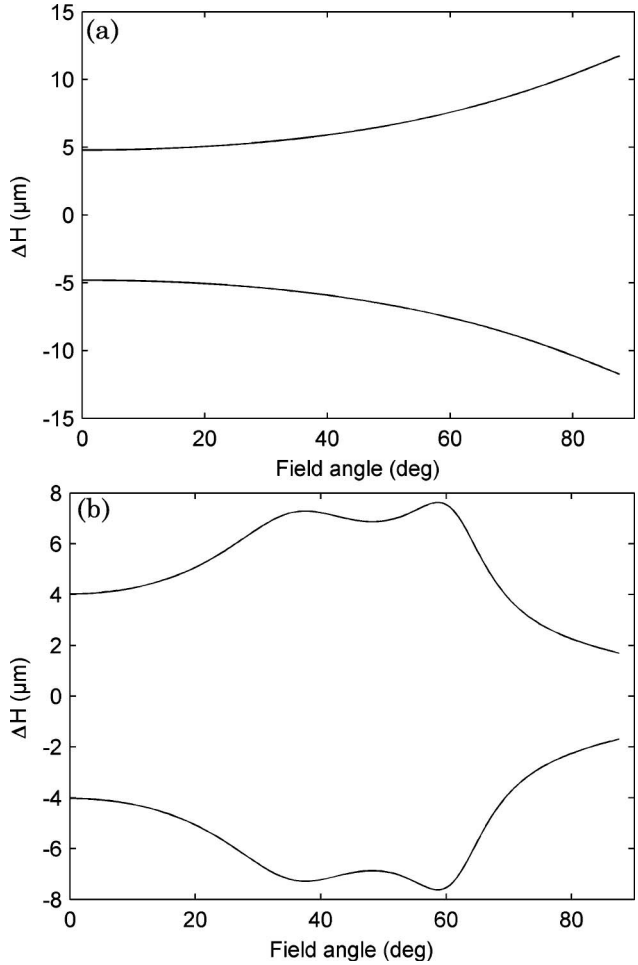


Fig. 7. Resulting envelope curves showing the displacement of the image caused by a constant slope error. This displacement depends on the field angle in both lenses. (a) For the FEL, moving the error toward the edge of the front lens worsens the displacement because the effects of increasing incidence angle more than counterbalance the decreasing local focal length. (b) For the PML, because the effects of increasing incidence angle are less important than changes in local focal length, the produced displacement is shaped in great part by the local focal length or, in other words, the impacts are worse where the resolution is higher.

also increasing. Finally, since the surface normal increases with the field of view, a given constant surface error $\partial Z_{\text{error}}/\partial Y$ tends to produce decreasing angle $\alpha$, an effect of using an error along the $z$ axis instead of normal to the surface. The combination of these three effects is seen using Eq. (7) to obtain an envelope curve for a given constant surface slope error $\partial Z_{\text{error}}/\partial Y$ of 0.00529, a value representing the maximum slope of a Gaussian surface shape having an amplitude of 10 $\mu$m and a FWHM of 6 times the 0° entrance pupil diameter, or 2.7 mm. These values for the error are chosen to show effectively the displacement and allow a direct comparison to the results from Fig. 3. The resulting curve is presented at Fig. 7(a), showing that, for the front lens of the FEL, a given surface error will have a greater impact near the edges than around the center. In this particular lens, the effect of the local focal length is more than counterbalanced by the increasing incident angle, explaining the difference between Figs. 6(a) and 7(a).

The same kind of analysis can quickly be done for any lens, but for compactness, only one other case is presented here, the case of a PML. This lens is designed to have a given resolution curve depending on the observation angle, having a maximum resolution around 63°, as seen on the curve of the local focal length in Fig. 6(b). This lens has a lot of controlled distortion produced by the first surface of the system and is chosen to show the impact of a rapidly changing local focal length. Since the PML is also a wide-angle lens, large incidence and normal angles relative to the optical axis are present and a combination of the three previously described factors using Eq. (7) is shown in Fig. 7(b), where the curve is obtained for a given constant error of 0.0070, again a value representing the maximum slope of a Gaussian error of 10 $\mu$m and having a FWHM of 6 times the entrance pupil diameter, or 2.04 mm. This time, the shape of the curve is mainly influenced by the local focal

length from Fig. 6(b), while the effect of increasing incidence angle explains the remaining difference.

## 4. Discussion

### A. Setting Manufacturing Tolerances

It can be useful to know how a given surface error will affect the image displacement for various positions on the lens, but the real use of this approach is to invert Eq. (7) to find a limiting acceptable error at each position of the surface, given a maximum acceptable $\Delta H$, expressed in a number of pixels or in micrometers. This is easily done when using the approximate Eq. (4) for small angles, but has to be evaluated numerically if using the complete Eq. (3). Because the term $(\theta - \varphi_N)$ is of the order of 1 rad near the edge for both systems presented in this paper, the series expansion does not converge fast enough and the real equation is used. Setting a maximum allowed image displacement of 10 $\mu$m (about 2 pixels for a VGA sensor), the two curves of Fig. 8 are obtained. It is interesting to see that, for the FEL, the tolerances have to be tightened when going toward the edge of the front lens surface to remain in the acceptable maximum image shift. As for the PML, because of the particular curve for the local focal length, it can be seen that the region where tight tolerances are important is between 30° and 70°, and that larger slope errors are acceptable near the edge.

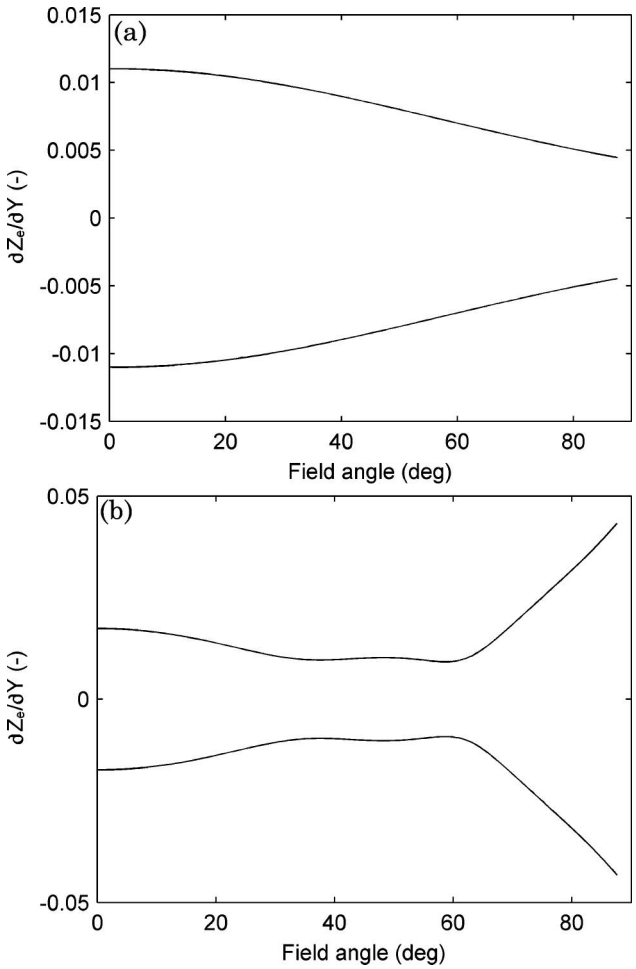


Fig. 8. Maximum allowed surface error slopes versus the field angle to achieve a constant image height displacement of 10 $\mu$m. (a) For the FEL, the edge is the most critical region. (b) For the PML, the most critical region is near the maximum of resolution of around 60°.

The main observation here is that each lens system is particular and some regions of the lenses have to be toleranced more tightly in terms of maximum surface error slope, while other regions can allow looser tolerances. For a given IRR amplitude, the maximum permitted surface slope will set the maximum spatial frequency of the IRR. For some fabrication methods of the lens, setting tolerances by region instead of for the whole lens can lead to cost reductions or easier fabrication methods. Consequently, it is highly desirable to consider the effect of the local focal length.

### B. Validity of the Approximations

When examining how accurate the previous model is, two things have to be considered. First, how accurate is the resulting $\Delta H$ for the chief rays and, then, how precise is it to approximate the surface seen by a bundle of rays by a small angle prism?

The resulting envelope curve for both lens systems has been compared to previous results obtained by adding known surface errors as grid sag surfaces in Zemax. For both lenses, the envelope curve fits almost perfectly with previously predicted values of $\Delta H$ using exact ray tracing. This can be seen for the PML by comparing the values around the maximum slope of each Gaussian error from Fig. 3 to the resulting envelope curve in Fig. 7(b) and noting how well it superposes.

By applying the same procedure on another surface during lens construction, the model does not work as perfectly as on the front surface. However, it is important to understand that the front surface, the one for which the equations in Subsection 3.A have been developed, is the most important surface to tolerance using the approach presented in this paper for wide-angle lenses. This is because the front surface produces the vast majority of the distortion in most of these lenses. It is also the one where aspheric surfaces are often used and the one on which the entrance pupil is often the smallest compared to the whole surface diameter. For a more general model valid for every surface of the system, not only the $\Delta\theta$ caused by the errors has to be considered, but also the fact that, if there were other optical surfaces before, a $\Delta\theta$ on the considered surface would also displace in the $Y$ direction where the chief ray hits this surface. This can easily be scripted in optical design programs for a more general approach for lenses that are not wide angle, but that are also affected by the problems discussed in this paper.

For the hypothesis that the error on the front surface is a small wedge producing only distortion equally for the whole bundle of rays at a given field

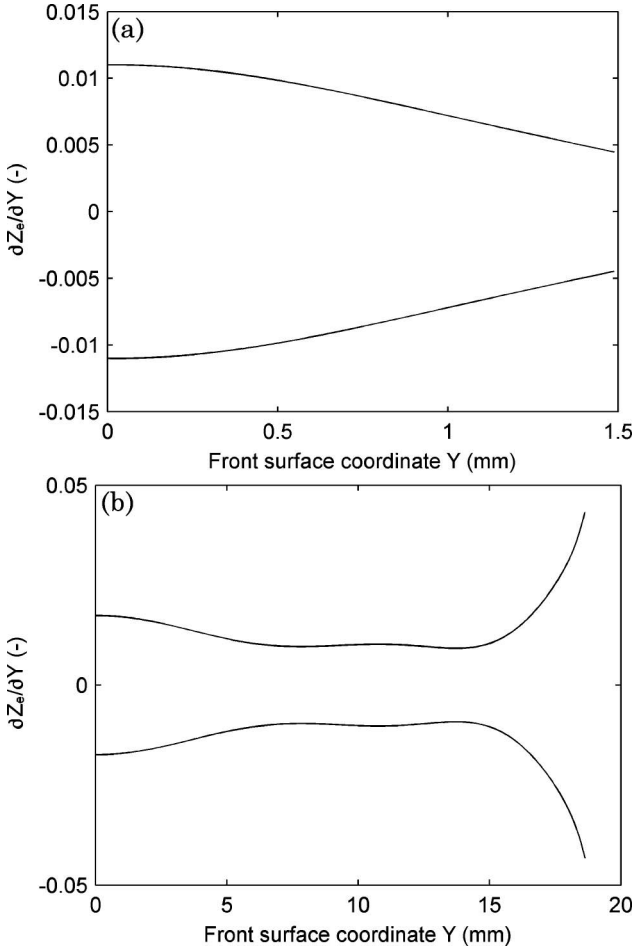


Fig. 9. Maximum allowed surface error slopes versus the lens coordinate $Y$ to achieve a constant image height displacement of 10 $\mu$m. Both curves are similar to Fig. 8, the difference coming from the nonlinear relation between $Y$ and $\theta$. (a) For the FEL and (b) for the PML.

angle, this is, of course, an approximation. When the spatial period of the IRR (inverse of the spatial frequency) becomes smaller than the beam footprint, other aberrations than distortion start to appear. Small localized surface errors can produce field curvature and astigmatism if the curvature of these errors is significant. They can be considered important when this curvature exceeds $\lambda/4$ peak to valley within the entrance pupil. To calculate if this $\lambda/4$ is exceeded, the curvature of the error can be related to the second derivative, but what must also be considered is the size of a bundle of rays on the front surface, which is affected by the entrance pupil variations [8].

### C. Links between Field Angle and Surface Coordinate

In the previous sections, the independent variable was the field angle $\theta$. However, when manufacturing a specific lens, the relation between lens coordinates $Y$ and the field angle $\theta$ is unknown and knowledge of the full system is required. In other words, the correspondence between $Y$ and $\theta$ has to be determined in the optical design application. The primary reason for this is that, for wide-angle lenses, the entrance pupil is considerably displaced away from the optical axis for increasing field angle, and this displacement is greatly determined by the local focal length curve $f(\theta)$, as shown in previous work [8]. Because of this unpredictable displacement of the entrance pupil, the paraxial magnification cannot be used to link the height $H$ on the image surface to the height $Y$ on the first surface. However, this is not really a drawback because, when an optical system is designed using a lens design program, the designer already knows where the chief ray at a given field angle will hit each surface because of the ray-tracing abilities of these programs. For the two lenses presented in this paper, the link between the field angle and the lens coordinate has been obtained in Zemax and the resulting maximum tolerance curves, similar to Fig. 8, are presented in Fig. 9, using lens units instead of field angle units as the horizontal axis.

## 5. Conclusion

The front lens of a panoramic imager is full of particularities. Not only does it produce the majority of the distortion needed in this kind of system to image a large field of view on an image plane, it is also a surface on which small localized errors can have major impacts. As presented in Subsection 3.A, a small angular error on this surface will have an impact that depends on three factors: the local focal length, the surface normal, and the angle of incidence at the location of this error. All of these are combined in Eq. (7) for the final displacement in the image for any surface error. This equation shows that, for panoramic lenses, there are regions on the surface where errors are more critical than others, thus allowing us to define zones of tighter tolerances versus other zones on the same lens surface. For the FEL, this zone of highest tolerance is near the edge of the lens, while, for the PML, this zone is around 60°, the maximum of the local focal length (resolution) curve.

The results presented show that the surface IRR error is not efficient for specifying surface error on an optical surface when the entrance pupil diameter is small relative to the lens diameter. In such a case, the dominant error is the slope or gradient of the surface error and it produces an image deformation. Moreover, we show that the impact of the slope error is spatially dependent. Consequently, when designing particular lenses, such as wide-angle ones, it is important to use appropriate error functions in order to fully determine the optical component's specifications.

The proposed approach is not limited to panoramic lenses. Many optical systems have a tight distortion requirement and a small exit or entrance pupil. Off-axis mirrors in a head-mounted display or a high-resolution spectrograph may benefit from our approach.

This research was supported by the Natural Sciences and Engineering Research Council of Canada.

## References


1. J. S. Chahl and M. V. Srinivasan, "Range estimation with a panoramic visual sensor," J. Opt. Soc. Am. A **14**, 2144–2151 (1997).
2. G. Jang, S. Kim, and I. Kweon, "Single-camera panoramic stereo system with single-viewpoint optics," Opt. Lett. **31**, 41–43 (2006).
3. T. J. Herbert, "Calibration of fisheye lenses by inversion of area projections," Appl. Opt. **25**, 1875–1876 (1986).
4. M. C. Sanson, C. T. Tienvieri, and S. VanKerkhove, "Localized slope errors and their impact on image performance requirements," in *International Optical Design*, OSA Technical Digest Series (CD) (Optical Society of America, 2006), paper ThB2.
5. S. Thibault, "IR panomorph lens imager and applications," Proc. SPIE **6940**, 69401A (2008).
6. G. Erdei, J. Fodor, P. Kallo, G. Szarvas, and F. Ujhelyi, "Design of high-numerical-aperture Fourier objectives for holographic memory card writing/reading equipment," Proc. SPIE **4093**, 464–473 (2000).
7. K.-L. Huang, "The tolerance analysis of wide-angle lens," Proc. SPIE **5638**, 976–985 (2005).
8. J. Parent and S. Thibault, "Tolerancing panoramic lenses," Proc. SPIE **7433**, 74330D (2009).
9. G. Erdei, G. Szarvas, and E. Lörincz, "Tolerancing surface accuracy of aspheric lenses used for imaging purposes," Proc. SPIE **5249**, 718–728 (2004).
10. J. K. Lawson, D. M. Aikens, R. E. English, W. T. Whistler, W. House, and M. A. Nichols, "Surface figure and roughness tolerances for NIF optics and the interpretation of the gradient, P-V wavefront, and RMS specifications," Proc. SPIE **3782**, 510–517 (1999).
11. R. H. Wilson, R. C. Brost, D. R. Strip, R. J. Sudol, R. N. Youngworth, and P. O. McLaughlin, "Considerations for tolerancing aspheric optical components," Appl. Opt. **43**, 57–66 (2004).
12. W. J. Smith, *Modern Optical Engineering*, 4th ed. (McGraw-Hill, 2007).